DNA Nanotechnology: From Sensing and DNA Machines to Drug-Delivery Systems

Chun-Hua Lu, Bilha Willner, and Itamar Willner*

Institute of Chemistry and The Center for Nanoscience and Nanotechnology, The Hebrew University of Jerusalem, Jerusalem 91904, Israel

This Perspective is contributed by a recipient of the 2013 *ACS Nano* Lectureship Awards, presented at the International Conference on Nanoscience & Technology, China 2013 (ChinaNANO 2013) in September 2013. The *ACS Nano* Lectureship honors the contributions of scientists whose work has significantly impacted the fields of nanoscience and nanotechnology.

ABSTRACT DNA/nanoparticle hybrid systems combine the unique electronic and optical properties of nanomaterials with the recognition and catalytic properties of nucleic acids. These materials hold great promise for the development of new sensing platforms, the programmed organization of nanoparticles, the switchable control of plasmonic phenomena in the nanostructures, and the controlled delivery of drugs. In this Perspective, we summarize recent advances in the application of DNA/nanoparticle (NP) hybrids in these different disciplines. Nucleic acid—semiconductor quantum dot hybrids are implemented to develop multiplexed sensing platforms for targeted DNA. The chemiluminescence resonance energy transfer mechanism is introduced as a new transduction signal, and the amplified detection of DNA targets through the biocatalytic regeneration of analytes is demonstrated. DNA machines consisting of catenanes or tweezers, and modified with fluorophore/Au NP pairs are used as functional devices for the switchable "mechanical" control of the fluorescence properties of the fluorophore. Also, nucleic acid nanostructures act as stimuli-responsive caps for trapping drugs in the pores of mesoporous SiO_2 nanoparticles. In the presence of appropriate biomarker triggers, the pores are unlocked, leading to the controlled release of anticancer drugs. Selective cancer-cell death is demonstrated with the stimuli-responsive SiO_2 nanoparticles.

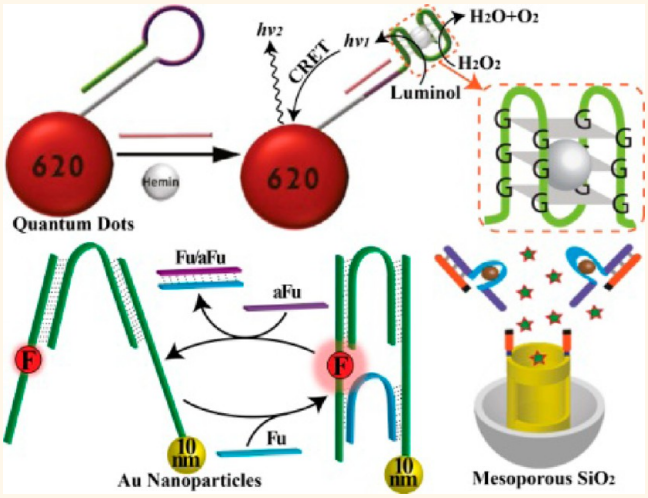

KEYWORDS: quantum dot · chemiluminescence resonance energy transfer (CRET) · sensor · nanocluster · graphene oxide · nanoparticle · plasmon · fluorescence · DNA machine · tweezers · catenane · mesoporous · stimuli-responsive · drug delivery · controlled release · chemotherapy · cancer cells

The base sequences of DNA encode substantial structural and functional information into the biopolymer. Besides the duplex formation of nucleic acids, which dictates strand displacement and strand migration processes within the DNA duplexes,[1,2] the self-assembly of supramolecular nanostructures, such as G-quadruplexes,[3,4] i-motif,[5] or metal-ion-bridged duplex nucleic acids structures,[6,7] is controlled by the base sequences comprising the biopolymers. Functional information encoded in DNA includes the sequence-specific binding of proteins, sequence-controlled reactivity toward enzymes (nicking enzymes, endonucleases), specific recognition of low-molecular-weight substrates or macromolecules (by aptamers),[8,9] and sequence-controlled catalytic properties (DNAzymes).[10,11] The rich structural and functional properties of nucleic acids provide the basis for the rapidly developing area of DNA nanotechnology.[12,13] Different research directions in the area of DNA nanotechnology may be identified, and these include the use of the recognition and catalytic properties of nucleic acids for

* Address correspondence to willnea@vms.huji.ac.il.

Published online September 26, 2013
10.1021/nn404613v

sensing;[14,15] the self-assembly of one-, two-, and three-dimensional DNA nanostructures;[16,17] the use of DNA for the bottom-up construction of nanodevices;[18] the development of DNA machines;[19] and the application of nucleic acids as functional materials for biocomputing.[20,21] Different applications of DNA-based nanotechnological systems included the development of sensitive sensing platforms[22] (clinical diagnostics, analysis of pathogen-causing diseases, biomarkers, detection of genetic disorders, environmental control, homeland security, and forensic applications), the development of intracellular autonomous sense-and-treat systems,[23] and the use of DNA matrices as drug carrier and release systems.[24] In this Perspective, we highlight one facet of our research efforts in the area of DNA nanotechnology, namely, the organization of tailored DNA–nanoparticle hybrids as functional systems for ultrasensitive sensing, for controlling plasmonic properties, and for the controlled delivery and release of drugs.

Semiconductor quantum dots (QDs) exhibit unique photophysical properties, such as high luminescence quantum yields, size-controlled luminescence properties, narrow luminescence bands and large Stokes shifts, and stability toward photobleaching.[25,26] Substantial research efforts were directed toward the application of surface-modified QDs for optical and photoelectrochemical sensing and biosensing.[27,28] We have recently implemented semiconductor QDs modified with the hemin/G-quadruplex horseradish-peroxidase-mimicking DNAzyme as a versatile sensing material, using chemiluminescence resonance energy transfer (CRET) as a readout signal. The hemin/G-quadruplex horseradish-peroxidase-mimicking DNAzyme has been used as a colorimetric,[29] chemiluminescent,[30] and electrocatalytic[31] label for different DNA- or aptamer-based sensing platforms. We found that the hemin/G-quadruplex-catalyzed oxidation of luminol by H_2O_2 yields chemiluminescence (λ = 430 nm), exhibiting a luminescence spectrum that overlaps the absorbance bands of different sized CdSe/ZnS QDs.[32] Accordingly, the chemiluminescence process provides an energy source for the excitation of the QDs, thus triggering their excitation without an external light source. Accordingly, the CRET-based analysis of DNA, using hemin/G-quadruplex–QDs conjugates, was demonstrated. Semiconductor QDs (λ_{em} = 620 nm) were modified by a hairpin probe, **1**, that included the target recognition sequence and the G-quadruplex DNAzyme sequence that was caged in a catalytically inactive configuration in the stem region of the hairpin, Figure 1A. In the presence of the target DNA, **2**, and hemin the hairpin structure was opened, thus releasing the G-quadruplex sequence that self-assembled into the hemin/G-quadruplex DNAzyme structure. The DNAzyme catalyzed the oxidation of luminol by H_2O_2-generating chemiluminescence, and the resulting CRET process triggered the luminescence of the QDs, Figure 1B. As the CRET process is controlled by the amount of opened hairpins and active DNAzyme, the resulting CRET signal relates to the concentration of the target DNA, and it provides a quantitative readout signal for analyzing the target DNA, Figure 1B, inset. With the use of three different sized QDs, the multiplexed analysis of three different DNA targets was demonstrated, Figure 1C. Three different sized QDs (λ_{em} = 620 nm, λ_{em} = 560 nm, and λ_{em} = 490 nm) were functionalized with three different hairpins, **1**, **3**, and **4**. Each of the hairpins included a specific recognition sequence for the targets **2**, **5**, and **6**, respectively, and the stem region of all hairpins included the G-quadruplex sequence in a catalytically inactive, caged, configuration. In the presence of the respective targets (**2**, **5**, **6**), and any mixture of the targets, their multiplexed analysis was demonstrated, Figures 1D and E. That is, the target(s) selectively opened the hairpin probes associated with the respective QDs, leading to the activation of the luminescence with the respective QDs. This CRET-based analytical platform enabled the analysis of DNA with a detection limit of 1×10^{-8} M, and the method was extended to develop aptamer-substrate sensing platforms, and sensors for the detection of hazardous metal ions (Hg^{2+}).[33]

In this Perspective, we highlight one facet of our research efforts in the area of DNA nanotechnology, namely, the organization of tailored DNA–nanoparticle hybrids as functional systems for ultrasensitive sensing, for controlling plasmonic properties, and for the controlled delivery and release of drugs.

The amplified detection of DNA is, however, a major challenge in bioanalysis. Toward this goal, one may use QDs not only as optical labels, but also as nanoscale carriers of probes. Indeed, amplified multiplexed detection of DNA was demonstrated with different sized QDs, utilizing the specific interactions between Exonuclease III (Exo III) and duplex DNA structures,[34] Figure 2A. The Exo III catalyzes the sequential hydrolytic cleavage of the 3′-end of the strand associated with a duplex DNA. The analytical platform made use of Exo III-catalyzed digestion of a DNA recognition complex as a means to regenerate the analyte,

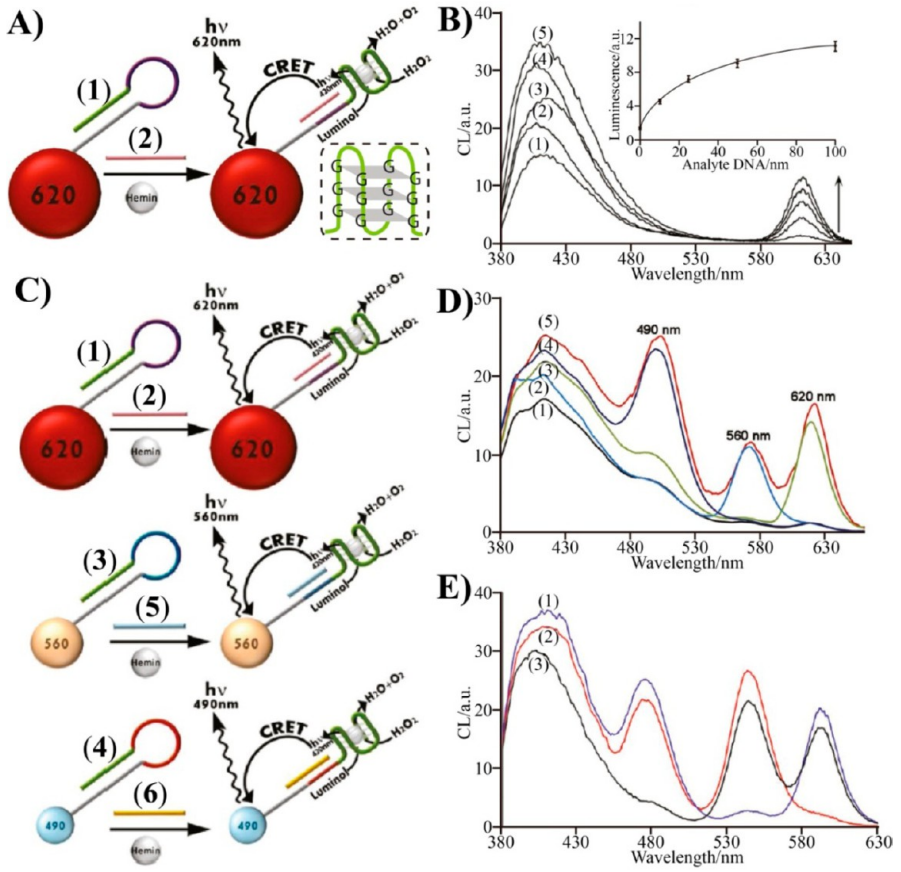

Figure 1. (A) Application of hairpin-functionalized CdSe/ZnS quantum dots (QDs) and the chemiluminescence resonance energy transfer (CRET) mechanism for analyzing target DNA. Opening of the hairpin structure upon the binding of the target leads to the self-assembly of the hemin/G-quadruplex that stimulates the CRET process. (B) Luminescence spectra generated by the hemin/G-quadruplex-stimulated CRET process upon analyzing different concentrations of the target DNA. Inset: Calibration curve corresponding to the CRET-stimulated luminescence intensities of the QDs in the presence of variable concentrations of the target DNA. (C) Multiplexed analysis of three different target DNAs by three different sized CdSe/ZnS QDs modified with three hairpins that include specific recognition sites for the targets, and the G-quadruplex sequence in a caged inactive configuration. (D) Luminescence spectra corresponding to the mixture of the three-sized CdSe/ZnS QDs: (1) in the absence of any target; (2) in the presence of target 5; (3) in the presence of target 2; (4) in the presence of target 6; (5) in the presence of a mixture of the three targets (2, 5, 6). (E) Multiplexed analysis of two target mixtures by the three, different sized, hairpin-functionalized QDs: (1) a mixture of targets 2 and 6; (2) a mixture of targets 5 and 6; (3) a mixture of targets 2 and 5. Reprinted from ref 32. Copyright 2011 American Chemical Society.

thereby providing an amplification path. Accordingly, two different sized CdSe/ZnS QDs, emitting at $\lambda_{em} = 540$ and 620 nm, were modified with probe nucleic acids **7** and **8** that included recognition sequences for the analytes **9** and **10**, respectively. Each of the recognition sequences was modified at its 3′-end with the black-hole quenchers (BHQ-1 or BHQ-2), leading to the quenching of the luminescence of any of the two-sized QDs. In the presence of the targets **9** or **10** (or a mixture of them) and Exo III as an auxiliary biocatalyst, the formation of the recognition complexes **7**/**9** or **8**/**10** was followed by the Exo III-catalyzed cleavage of the probe strands **7** and/or **8**, leading to the separation of the BHQ units. The catalytic digestion of the probe strand(s) led to the regeneration of the targets for their continuous hybridization with the probes and the subsequent cleavage of the probe units associated with the QDs. The separation of the BHQ units triggered the luminescence of the respective QDs, thus allowing the multiplexed analysis of the targets **9** and **10**, Figure 2B. The regeneration of the target-analytes enabled the analysis of the targets with a detection limit corresponding to 1×10^{-12} M. The concept of using Exo III as a biocatalyst for the regeneration of the target-analyte was further implemented to develop amplified aptasensors (*e.g.*, the detection of the vesicular epithelial growth factor, VEGF, being a biomarker for Alzheimer's disease[35]).

The recently discovered nucleic-acid-stabilized metal nanoclusters (NCs) provide an additional approach to develop multiplexed DNA sensors and aptasensors.[36] It was found that specific nucleic acid sequences stabilize metal NCs that exhibit luminescence properties (*e.g.*, Ag NCs). The luminescence features of these NCs are controlled by the sizes of the metal aggregates and by the sequences of the stabilizing capping oligonucleotides. The sensing

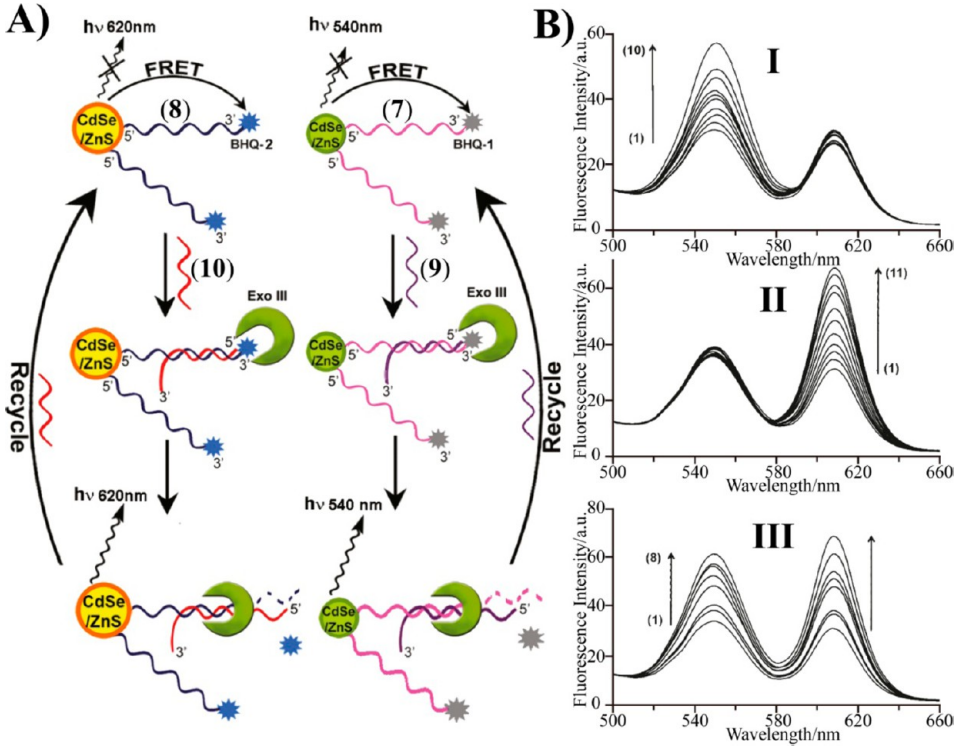

Figure 2. (A) Multiplexed amplified analysis of two target DNAs using two different sized semiconductor quantum dots (QDs) and the Exo III-catalyzed regeneration of the DNA targets as amplification routes. (B) Time-dependent luminescence spectra of the system consisting of the two sized QDs upon analyzing: (I) target 9; (II) target 10; (III) the mixture of targets 9 and 10. Reprinted from ref 34. Copyright 2011 American Chemical Society.

platform[37] made use of the fact that single-stranded nucleic acids adsorb onto graphene oxide (GO) while duplex structures of DNA desorb from the GO matrices. Accordingly, the red-emitting Ag NCs, λ_{em} = 616 nm, were stabilized with the nucleic acid **11**, consisting of the sequence stabilizing the NCs and the sequence recognizing the immunodeficiency virus gene, HIV. Similarly, the near-infrared-emitting Ag NCs, λ_{em} = 775 nm, were stabilized with the nucleic acid **12**, comprising the specific sequence stabilizing the NCs and elongated by the sequence recognizing the hepatitis B, HBV gene. The Ag NCs-functionalized probes **11** and/or **12** were adsorbed onto GO, leading to the quenching of the luminescence of the respective Ag NCs, Figure 3A. Subjecting the **11**- and/or **12**-functionalized GO to the HIV gene (**13**) or the HBV gene (**14**) resulted in the desorption of the respective recognition duplexes **11**/**13** and/or **12**/**14**, and the recovery of the luminescence properties of the respective Ag NCs. The luminescence intensities of the red-emitting Ag NCs, upon analyzing different concentrations of the HIV gene (**13**), and the luminescence intensities of the near-infrared-emitting Ag NCs, upon analyzing different concentrations of the HBV gene (**14**), and the respective calibration curves are shown in Figures 3B and C. The multiplexed analysis of the two genes is exemplified in Figure 3D.

Another rapidly developing area in DNA nanotechnology involves the construction of DNA machines.[19] A molecular DNA machine has several basic properties: (i) the molecular device performs "mechanical" functions such as translocation or rotation; (ii) the mechanical process requires a fuel-input; (iii) the mechanical operation is accompanied by an energy consumption reaction that yields waste products; and (iv) for the reversible and cyclic operation of a DNA device, the introduction of "antifuel" triggers motion that opposes the fueled mechanical transitions. Recently, different DNA machines, such as tweezers, walkers, gears, cranes, interlocked catenanes, and more, were designed. Different fuels and antifuels were implemented to activate the devices, and these included nucleic acid strands and antistrands,[38] pH (H^+/OH^-),[39] metal-ions and binding ligands (Hg^{2+}/cysteine),[40] and light.[41] Different applications of DNA machines were suggested, including the transport of cargoes by nanorobots,[42] the programmed assembly of nanoparticles,[43] and the monitoring of intracellular processes.[44,45] The dynamic and reversible control of the distances separating functional units associated with DNA machines suggests, however, that spatially controlled physical phenomena, such as plasmonic effects, could be switched by DNA devices.

While metallic nanoparticles usually act as quenchers of fluorophores, at certain distances separating the fluorophore and nanoparticle, surface-enhanced fluorescence (SEF) is observed. The distance region at

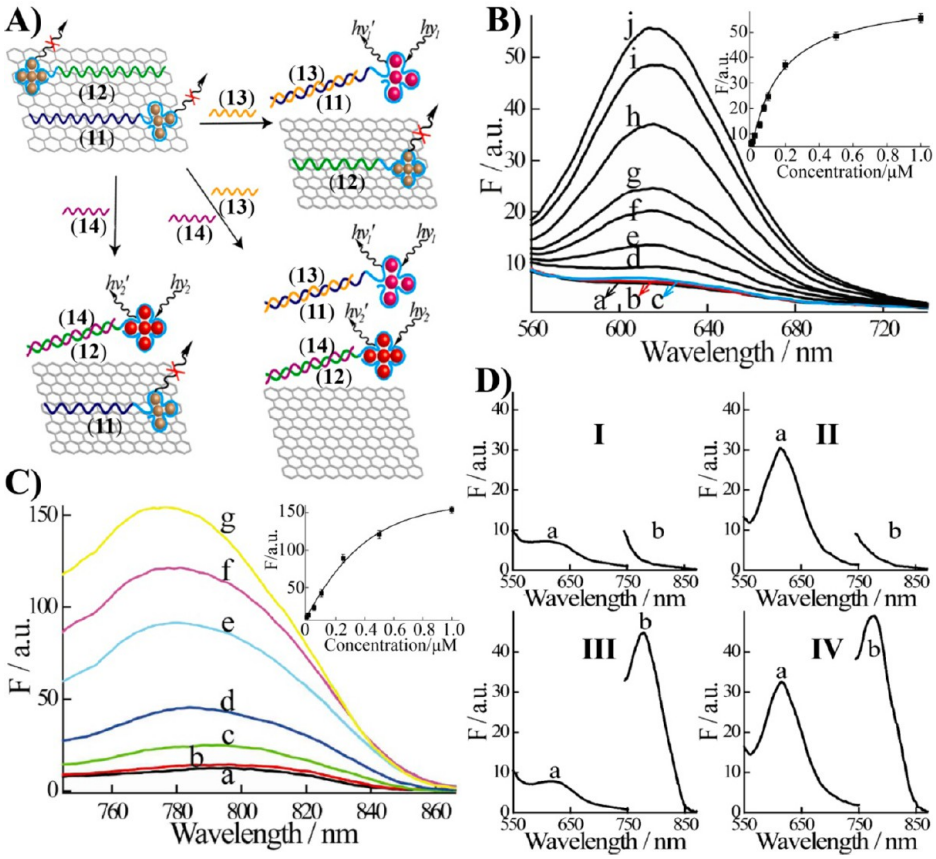

Figure 3. (A) Implementation of two different luminescent nucleic acid-stabilized Ag nanoclusters associated with graphene oxide (GO) for the multiplexed optical analysis of the HIV and HBV genes. (B) Luminescence spectra corresponding to the desorbed red-emitting Ag nanocluster duplexes, upon analyzing different concentrations of the HIV gene. Inset: The resulting calibration curve. (C) Luminescence spectra corresponding to the desorbed near-infrared-emitting Ag nanocluster duplexes, upon analyzing different concentrations of the HBV gene. Inset: The resulting calibration curve. (D) Luminescence spectra generated by the graphene oxide functionalized with the red-emitting and near-infrared-emitting Ag nanocluster (NC) probes, 11 and 12: (I) in the absence of the targets; (II) in the presence of the HIV gene; (III) in the presence of the HBV gene; (IV) in the presence of the HIV and the HBV genes. The concentrations of the target genes corresponded to 100 nM, and the luminescence spectra were recorded after a fixed time interval of 80 min of desorption of the Ag nanoclusters from the graphene oxide matrix. Reprinted from ref 37. Copyright 2013 American Chemical Society.

which SEF occurs is controlled by several parameters, including the size of the NPs, the quantum yield of the fluorophores, the refractive index of the medium, the prolate aspect ratio, and the distance separating the fluorophore/metal nanoparticle. Theoretical modeling of the fluorescence quantum yields as a function of fluorophore–nanoparticle separation distances is feasible,[46] and correlation between theory and experimental results is possible. For example, switchable fluorescence/plasmonic NPs interactions were observed by tethering a fluorophore and a plasmonic Au NP to different positions of DNA tweezers devices, and by controlling the distances separating the fluorophore/Au NP by means of the mechanical operation of the tweezers.[47] For example, the tweezers T_1 and T_2, depicted in Figures 4A and B were examined as molecular devices for the plasmonic control of the fluorescence properties of a fluorophore. The tweezers T_1 shown in Figure 4A consists of two arms, **15** and **16**, bridged by the nucleic acid **17**. The arm **15** was modified at its 3′-end with a fluorophore, while the 5′-end of arm **16** was functionalized with a 10-nm Au NP. The tweezers in state I were closed by a fuel strand **18** to yield the closed tweezers state II, while the tweezers were reopened by the elimination of the bridging unit **18** using an antifuel strand **19**. Figure 4A, panel I, depicts the fluorescence changes of the system upon the cyclic closure and opening of the tweezers by the fuel and antifuel strands, respectively. While the closed tweezers, state II, reveals quenching of the fluorescence, the formation of state I leads to a higher degree of fluorescence. Figure 4A, panel II, depicts the theoretically calculated distance-dependent fluorescence quantum yields of the specific fluorophore (Cy3) in the presence of the 10-nm Au NP. The estimated distances separating the fluorophore/Au NP in the open and closed states of the tweezers are provided in Figure 4A. One may realize that the close distance separating the fluorophore/Au NP in state II, 1–2 nm, leads to efficient quenching of the fluorescence, as predicted theoretically, whereas the spatial separation between the fluorophore/Au NP

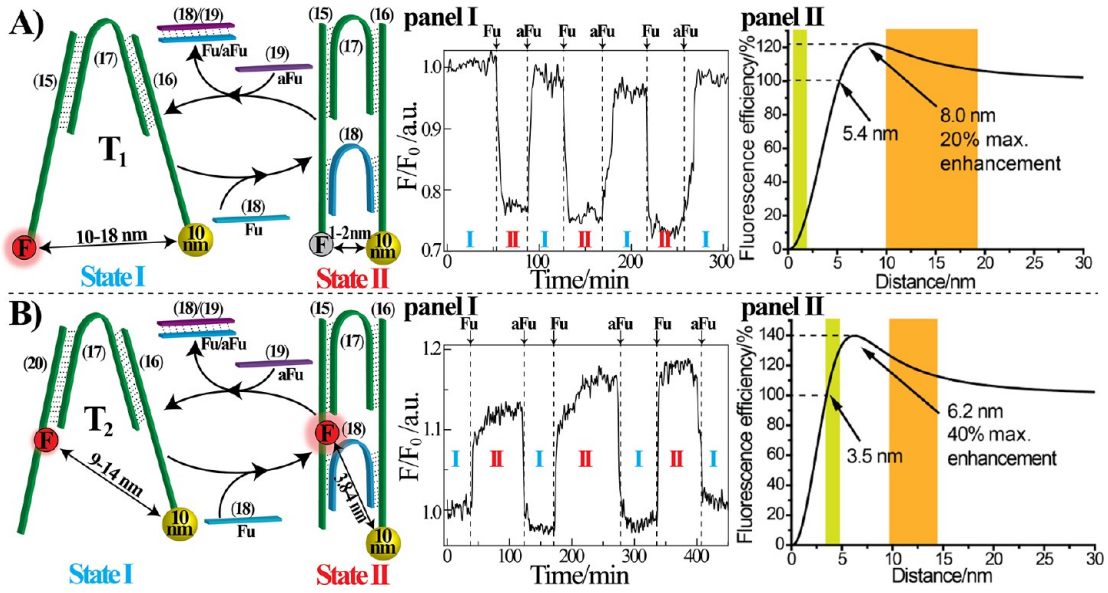

Figure 4. Mechanical switchable control of the fluorescence properties of a fluorophore, Cy3, using different DNA tweezers devices that include structurally dictated configurations of a 10-nm nanoparticle (NP) and the fluorophore, Cy3. The distance between the fluorophore and the Au NPs in the different tweezers is controlled upon the reversible fueled and antifueled closure and opening of the tweezers. (A) Tweezers T_1 consisting of the fluorophore and Au NP positioned at the ends of the arms 15 and 16. (I) cyclic fluorescence changes of the system upon subjecting the tweezers to the fuel (closure) and antifuel (opening) processes. The results demonstrate that the closure of the tweezers leads to fluorescence quenching of the fluorophore. (II) Theoretical modeling of the fluorescence quantum yields of the Cy3 fluorophore as a function of the separating distance. (B) Tweezers T_2 consisting of the fluorophore positioned in the middle of the arm 20 and the Au NP at the end of the arm 16. (I) Cyclic fluorescence changes of the system upon subjecting the tweezers to the fuel (closure) and antifuel (opening) processes. The results demonstrate that the closure of the tweezers leads to surface-enhanced fluorescence of the fluorophore. (II) Theoretical modeling of the fluorescence quantum yield of Cy3 as a function of the separating distance of the units in tweezers T_2. Reprinted from ref 47. Copyright 2013 American Chemical Society.

in the open configuration, state I, 10−18 nm, has little effect on the fluorescence quantum yield of the Cy3 fluorophore. In turn, in tweezers T_2, Figure 4B, the fluorophore (Cy3) is positioned in the middle of arm **20**, while the Au NP is tethered to the 5′-end of arm **16** and its position is unchanged. Closure and opening of the tweezers T_2 by means of the fuel and antifuel strands result in the fluorescence changes shown in Figure 4B, panel I. In contrast to tweezers T_1, the closure of tweezers T_2 to state II leads to an enhanced fluorescence quantum yield, as compared to the tweezers in the open configuration, state I. Figure 4B, panel II, shows the theoretically predicted distance-dependent fluorescence quantum yields for the tweezers containing the fluorophore Cy3 in an internal modified nucleic acid. The estimated separation distances of the fluorophore/Au NP in the closed and open T_2 tweezers states are 3.8−4.0 nm for the closed tweezers, state II, and 9−14 nm for the open tweezers T_2 in state I. The experimental results follow the theoretical predictions, and at a separation distance of *ca.* 3.5 nm, 20% fluorescence enhancement is expected, while at separation distances of 9−14 nm, the fluorescence quantum should not be affected.

> Another rapidly developing area in DNA nanotechnology involves the construction of DNA machines.

The switchable control of the fluorescence properties of fluorophore/Au NPs nanostructures by means of DNA machines was further demonstrated using the three-ring DNA catenane as the programming machine,[48] Figure 5A. The three-ring catenane system, consisting of rings α, β, and γ, was functionalized with a fluorophore (Cy3) on ring α and with a 10-nm Au NP on ring γ to yield the linear structure L_1. While the ring γ forms a stable duplex by the hybridization of domain I of ring γ with ring β, the domains II and III associated with ring α are sequence-equivalent and can also hybridize with parts of the sequence I associated with ring γ. The three-ring configuration L_1 is, however, the energetically favored nanostructure. The strand displacement of ring γ from ring β by means of a fuel strand triggers, in principle, two equiprobable translocations of ring γ, above or below the rims of ring β, to occupy the sites II and III on ring α. It was found, however, that blocking the lower rim of ring β by a nucleic acid blocker (B_1), dictates, in the presence of the fuel strand, the selective transition of ring γ across the upper rim of ring β to bind to site II of ring α, leading to the three-ring configuration M_1. Similarly, blocking the upper rim of

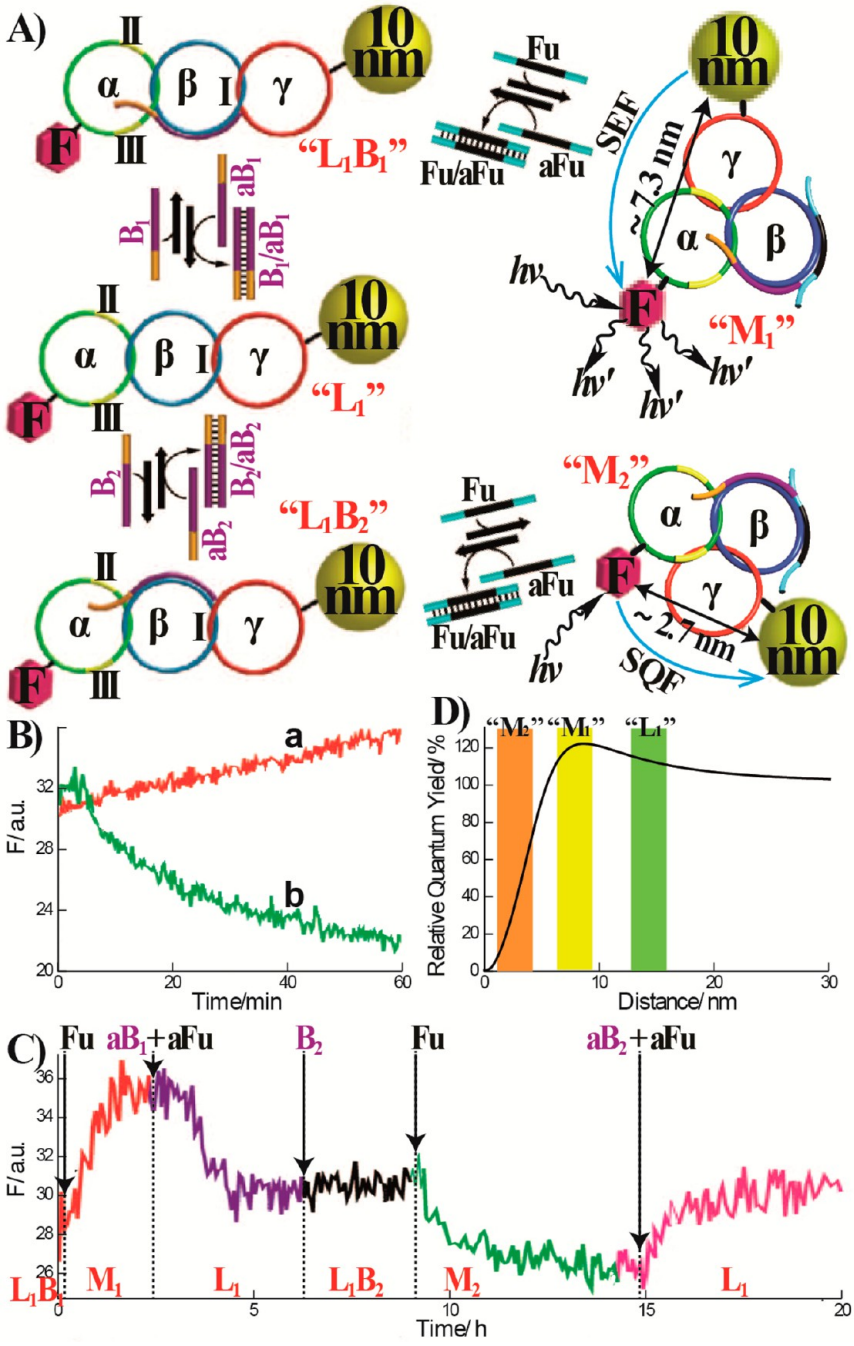

Figure 5. (A) Switchable fluorescence properties of the Cy3 fluorophore, stimulated by a three-ring catenane device functionalized with a 10-nm Au nanoparticle (NP) and a fluorophore (F = Cy3), upon the cyclic and reversible transition across the states L_1, M_1, and M_2, using the appropriate blocker/antiblocker and fuel/antifuel stands. (B) Time-dependent fluorescence changes upon reconfiguration of (a) structure L_1 to M_1 (implying fluorescence enhancement); (b) L_1 to M_2 (implying fluorescence quenching). (C) Time dependent fluorescence change upon the transitions $L_1 \rightarrow M_1 \rightarrow L_1 \rightarrow M_2 \rightarrow L_1$ in the presence of the appropriate blocker/antiblocker and fuel/antifuel. (D) Theoretical modeling of the fluorescence quantum yield as a function of the distance separating the Au NP/fluorophore pair. Bars indicate the estimated distance separating the fluorophore/Au NP in the different states. Reprinted with permission from ref 48. Copyright 2013 Nature Publishing Group.

ring β in configuration L_1 with a blocker unit (B_2), followed by the fuel-stimulated strand displacement of ring γ, results in the selective transition of ring γ along the lower rim of ring β to site III of ring α to form configuration M_2. Figure 5B, curve a, shows the time-dependent fluorescence changes upon the reconfiguration of structure L_1 to M_1. The increase in the fluorescence intensities indicates surface-enhanced fluorescence in the system. In turn, the rearrangement of structure L_1 into the structure M_2 is accompanied by a decrease in the fluorescence, Figure 5B, curve b, implying that this reconfiguration process leads to quenching of the fluorophore by the Au NP. By the cyclic treatment of the system with the appropriate

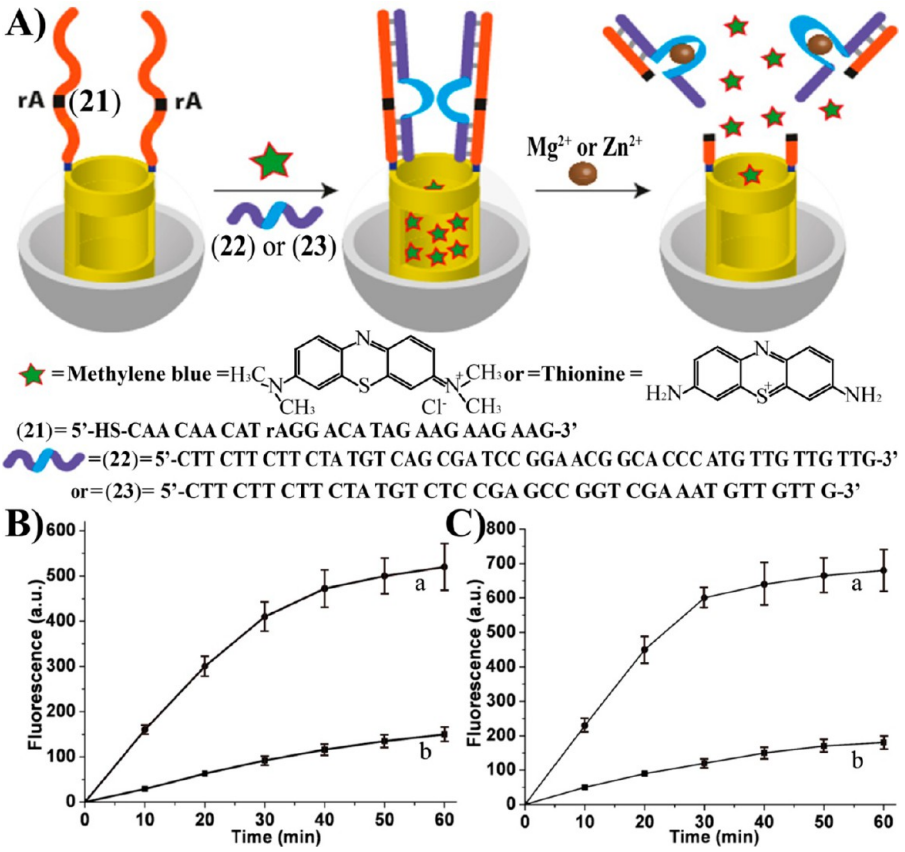

Figure 6. (A) Schematic locking of two fluorescent substrates, methylene blue, or thionine, in mesoporous SiO_2 nanoparticles (NPs), by means of DNA duplex caps, and the controlled release of the fluorescent substrates by the selective unlocking of the pores by fragmenting the DNA caps with the Mg^{2+}-dependent DNAzyme or the Zn^{2+}-dependent DNAzyme. (B) Time-dependent fluorescence changes observed upon (a) the Mg^{2+}-dependent DNAzyme-stimulated release of methylene blue from the pores; (b) background fluorescence changes corresponding to the leakage of methylene blue from the pores. (C) Time-dependent fluorescence changes observed upon (a) the Zn^{2+}-dependent DNAzyme-stimulated release of thionine from the pores; (b) background fluorescence changes corresponding to the leakage of thionine from the capped pores. Reprinted from ref 56. Copyright 2013 American Chemical Society.

blocker/antiblocker and fuel/antifuel strands, the fluorescence features of the system could be reversibly cycled between fluorescence enhancement and fluorescence quenching states, using the DNA catenane machine as a controlling scaffold, Figure 5C. The experimental results were further supported by theoretical modeling of the distance-dependent fluorescence quantum-yield efficiencies of the Cy3/10-nm Au NP system, Figure 5D. The distance separating the fluorophore/10-nm Au NP in configuration M_1 is estimated to be 7.3 nm, consistent with the observed enhanced fluorescence. In turn, in structure M_2, the distance separating the fluorophore/Au NP is estimated to be 2.7 nm, consistent with the observed fluorescence quenching. In structure L_1, the distance separating the fluorophore from the Au NP is *ca.* 14 nm, suggesting little effect on the fluorescence quantum yield of the fluorophore.

Finally, we address the implementation of hybrid DNA/mesoporous SiO_2 NPs as "smart" drug carriers and controlled release systems.[49] Mesoporous materials are the subject of growing interest as carriers and controlled release systems. The high surface area of porous materials enables both the effective loading of the pores and the locking of the substrates in the pores by stimuli-responsive gating caps. Different triggers to unlock the pores have been reported, including the use of pH,[50] light,[51] redox,[52] and enzymes[53] as pore-opening stimuli. Previous studies have implemented DNA-functionalized mesoporous SiO_2 NPs as stimuli-responsive matrices for the controlled release of substrates (drugs).[54,55] In these systems, the mesoporous NPs acted as containers for carrying and transporting the substrates, and the nucleic acids as stimuli-responsive gates that cap the pores and unlock them in the presence of appropriate input triggers. Figure 6A displays the principle of gating the release of fluorescent substrates (methylene blue [MB^+] or thionine [Th^+]) by means of metal-ion-dependent DNAzymes (the Mg^{2+}-dependent DNAzyme or the Zn^{2+}-dependent DNAzyme).[56] The pores of mesoporous SiO_2 NPs (diameter 50 nm) were functionalized with the nucleic acid sequence **21** acting as substrate for the Mg^{2+}-dependent DNAzyme

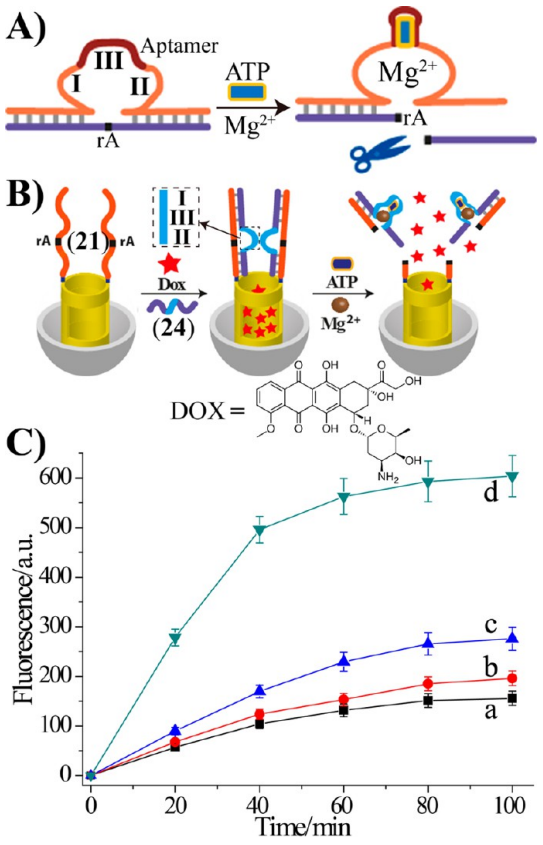

Figure 7. (A) The cooperative activation of the Mg^{2+}-dependent DNAzyme by the insertion of the aptamer sequence into the loop domain of the DNAzyme sequence, and the formation of the aptamer/adenosine triphosphate (ATP) biomarker complex. (B) The cooperative unlocking of the pores, associated with the mesoporous SiO_2 nanoparticles by means of the ATP/aptamer/Mg^{2+}-dependent DNAzyme units, resulting in the release of the anticancer drug doxorubicin from the pores. (C) Time-dependent release of doxorubicin from the mesoporous SiO_2 nanoparticles (NPs): (a) background release in the absence of Mg^{2+} ions and ATP; (b) in the presence of only ATP; (c) in the presence of Mg^{2+}-ions only; (d) in the presence of ATP and Mg^{2+}-ions. Adapted from ref 56. Copyright 2013 American Chemical Society.

and the Zn^{2+}-dependent DNAzyme. The pores were loaded with the fluorescent substrates, MB^+ or Th^+, and locked in the pores by the hybridization of the nucleic acid sequences **22** or **23**, corresponding to the Mg^{2+}- or Zn^{2+}-dependent DNAzyme sequences, with the substrate sequence **21**. In the presence of Mg^{2+} or Zn^{2+}, selective unlocking of the pores and programmed release of the fluorescent substrates were demonstrated, Figures 6B and C. These hybrid DNAzyme/SiO_2 NPs structures provide model systems for the ion-stimulated release of substrates from the pores. By further modification of the nucleic acid capping units, enhanced complexity of the unlocking mechanism of the pores was demonstrated, by designing nucleic acid caps that unlock the pores by cooperative DNAzyme/aptamer-substrate (biomarker) functionalities, Figure 7. This approach made use of the facts that: (i) insertion of a tandem oligonucleotide sequence into the specific DNAzyme sequence perturbs the catalytic functions of the metal-dependent DNAzyme due to the flexibility of the ion-binding loop, introduced by the foreign sequence; and (ii) intramolecular hybridization of the inserted foreign sequence or the formation of an aptamer–substrate complex, by the inserted sequence regenerates the DNAzyme activity, due to the rigidification of the ion-binding loop, Figure 7A. Realizing that extensive amounts of adenosine triphosphate (ATP) are generated in cancer cells due to the enhanced metabolism in these cells, we suggested that the ATP biomarker could be implemented as a functional component for the cooperative, DNAzyme-stimulated unlocking of the pores and the targeted release of an anticancer drug in cancer cells. Accordingly, the mesoporous SiO_2 NPs were modified with the Mg^{2+}-dependent DNAzyme substrate **21**, and the pores were loaded with doxorubicin (DOX), an anticancer drug. The drug was locked in the pores by the hybridization of the nucleic acid sequence **24**, which included two subunits I and II of the Mg^{2+}-dependent DNAzyme, and an insert sequence, III, that corresponded to the ATP-aptamer sequence, Figure 7B. Whereas in the presence of Mg^{2+}-ions and the absence of ATP inefficient opening of the pores was observed, Figure 7C, curve c, effective unlocking of the pores and the release of DOX were observed in the presence of both Mg^{2+} ions and ATP, Figure 7C, curve d. Preliminary experiments revealed that the DOX-loaded mesoporous SiO_2 underwent rapid endocytosis into cells. It was found that the Mg^{2+} ion content in the cells is sufficient to activate the DNAzyme-functionalized SiO_2 NPs and to unlock the pores. The excessive content of ATP generated in the cancer cells was found to trigger and to unlock the DOX-loaded SiO_2 NPs in cancer cells selectively, leading to their effective death. We find that after a time interval of 24 h, the death of 50% of the cancer cells was observed, while less than 10% of the normal cells were subjected to death. Control experiments supported the original paradigm that intracellular ATP indeed triggers the unlocking of the NPs and the release of the anticancer DOX drug. In these experiments, added oligomycin, which suppresses the intracellular generation of ATP, inhibited the death of the cancer cells.

A further approach to unlock nucleic-acid-capped, drug-loaded, pores of mesoporous SiO_2 has involved the

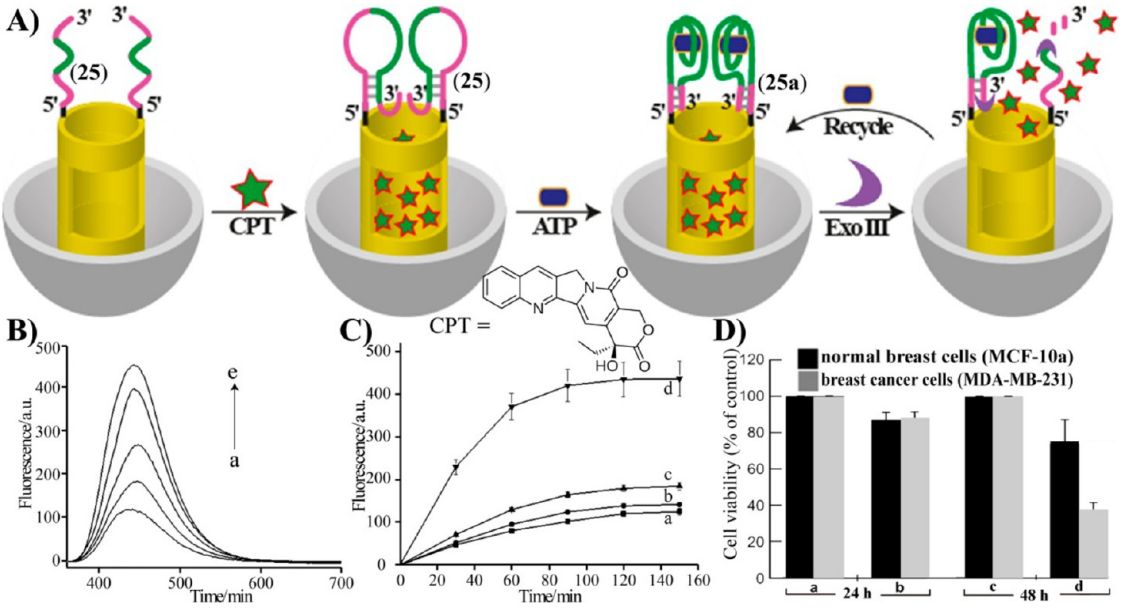

Figure 8. (A) Schematic unlocking of camptothecin- (CPT) loaded mesoporous SiO_2 nanoparticles (NPs) using adenosine triphosphate (ATP) as a trigger-biomarker, and Exo III as a cap-digestion biocatalyst. (B) Fluorescence spectra of CPT released in the presence of Exo III and variable concentrations of ATP after a fixed time interval of 60 min. ATP concentrations: (a) 0 mM; (b) 0.1 mM; (c) 0.5 mM; (d) 1 mM; (e) 2 mM. (C) Time-dependent fluorescence changes of released CPT: (a) background release in the absence of Exo III and ATP; (b) in the presence of ATP, 1 mM, and absence of Exo III; (c) in the presence of Exo III and the absence of ATP; (d) in the presence of Exo III and ATP, 1 mM. (D) Effect of CPT-loaded mesoporous SiO_2 NPs on the viability of normal breast cell (MCF-10a; black) and the breast cancer cells (MDA-MB-231; gray): (a) viability of the cells treated with CPT-unloaded SiO_2 NPs after 24 h; (b) viability of the cells loaded with the CPT after a time-interval of 24 h; (c) viability of the cells treated with the CPT-unloaded SiO_2 NPs after a time interval of 48 h; (d) viability of the cells treated with the CPT-loaded SiO_2 NPs after a time-interval of 48 h. Reprinted from ref 57. Copyright 2013 American Chemical Society.

The programmed cyclic reconfiguration of metallic nanoparticle structures, and particularly the spatial control of distances separating fluorophores and plasmonic nanoparticles by means of DNA machines, is a challenging new research area.

biocatalytic degradation of the nucleic acid by specific enzymes, such as endonucleases, nicking enzymes, or exonucleases.[57] This is exemplified in Figure 8A with the ATP-triggered unlocking of mesoporous SiO_2 NPs, loaded with the anticancer drug camptothecin (CPT), using exonuclease III (Exo III) as biocatalyst. The mesoporous SiO_2 NPs were functionalized with the nucleic acid **25**, which consisted of the ATP aptamer sequence and additional domains that could form an internal duplex hairpin structure. The thermal treatment of the NPs retained the nucleic acid **25** in the single-stranded configuration that allowed loading the pores with the anticancer drug CPT. Upon cooling the system, the nucleic acid units **25** reconfigured into the hairpin structure that capped and trapped CPT in the pores. The exonuclease III, Exo III, is a specific biocatalyst that sequentially digests only duplex DNA domains from the 3′-end. Realizing these properties of Exo III, the hairpin structure of **25** was designed to include a single-strand overhang, causing the hairpin units to be resistant to Exo III. In the presence of ATP, the hairpin structure, including the aptamer domain, rearranges into the aptamer–ATP complex, leading to an internal 3′-ended hairpin structure **25a**. The Exo III digestion of the 3′-end of the aptamer complex strand results in the separation of the aptamer–ATP complex and the release of ATP. This process activates the further degradation of capping hairpin units **25** by the ATP biomarker. That is, the Exo III-mediated cleavage of the **25a**/ATP structure regenerates the ATP biomarker, thus providing an amplification mechanism for the release of CPT. Figure 8B depicts the fluorescence intensities of the released CPT upon subjecting the CPT-loaded mesoporous SiO_2 NPs to different concentrations of ATP for a fixed time interval of 60 min in the presence of Exo III. As the concentrations of the ATP biomarker increase, the release of CPT is enhanced, implying that ATP indeed acts as a trigger to unlock the pores. Figure 8C depicts the time-dependent fluorescence changes as a result of releasing CPT from the pores. Realizing that the enzyme Endo GI, exhibiting Exo III type activities, is present in cancer cells, the effects of CPT-loaded mesoporous SiO_2 NPs capped with the ATP-responsive

hairpin **25** on MDA-MB-231 breast cancer cells and MCF-10a normal breast cells were examined, Figure 8D. After a time interval of 48 h, 65% cell death was observed for the MDA-MB-231 breast cancer cells, whereas only 25% cell death was encountered with the normal breast cells. Control experiments, using oligomycin as an inhibitor for the metabolic formation of ATP in cancer cells, demonstrated that the degree of cell death of the cancer cells decreased as the concentration of oligomycin increased. These results were consistent with ATP unlocking the pores and releasing the CPT anticancer drug.

This Perspective has addressed one facet of our activities in the area of nanobiotechnology. Specifically, we discussed recent advances in applying nucleic acid/nanoparticle hybrids for sensing applications, controlling switchable plasmonic functions by means of DNA machines, and the implementation of such hybrid systems for controlled drug release. Nucleic acid–NP composites combine the properties and functions of the hybrid components, thus providing new materials for different applications. Nucleic acid-functionalized QDs have enabled the introduction of a new sensing paradigm involving the CRET process. Also, amplified optical detection of DNA or aptamers through Exo III regeneration of the analytes was demonstrated. The size-controlled luminescence properties of QDs were then implemented for the multiplexed detection of analytes. A further new sensing platform has involved the integration of luminescent DNA-stabilized Ag NCs with GO as functional matrices for DNA sensing. By using nucleic acid-functionalized Ag NCs of different luminescence properties, multiplexed analysis of different DNA targets was achieved. By implementing other semiconductor QDs and by using other luminescent metal-DNA NCs (*e.g.*, Au, Cu), multiplexed analysis of enhanced complexities may be envisaged.

The programmed cyclic reconfiguration of metallic nanoparticle structures, and particularly the spatial control of distances separating fluorophores and plasmonic nanoparticles by means of DNA machines, is a challenging new research area. While solid theoretical modeling of the optical properties of ordered plasmonic nanoparticles or spatially organized fluorophore–nanoparticle assemblies is available, the correlation of theory with experimental systems remains limited. Specifically, plasmonic effects are anticipated to be enhanced with increasing nanparticle size. However, the synthesis of large metallic NPs that are modified with controlled numbers of nucleic acids, and particularly the stabilization of such particles against aggregation, encounters serious difficulties and limitations. Once general synthetic methodologies to prepare stable large plasmonic NPs with high yields are available, important new plasmonic phenomena in organized metallic NPs nanostructures can be envisaged. Finally, hybrids consisting of DNA and mesoporous nanoparticle materials hold great promise as drug carriers and autonomous sense-and-treat systems. The design of functional stimuli-responsive DNA caps for triggered unlocking of pores and controlled release of substrates (drugs) may provide a powerful new paradigm in nanomedicine. Specifically, precise aptamer sequences for biomarkers and catalysts (DNAzymes or enzymes) may act cooperatively as "smart" tools to unlock the pores and to release drugs. While important advances in applying stimuli-responsive mesoporous NPs for controlled drug release have been demonstrated, important challenges remain ahead of us. Mesoporous NP drug-delivery systems revealing enhanced functional complexities could be realized. For example, the biomarker-triggered release of a pro-drug and a drug activator from two different NP containers could be an interesting path to follow. Furthermore, understanding the basic mechanisms for endocytosis of NPs into cells, modification of NPs with cell-penetrating peptides and controlling their delivery into cells, as well as the use of different mesoporous nanoparticle materials (*e.g.*, carbon, TiO_2), are interesting subjects for further exploration.

Conflict of Interest: The authors declare no competing financial interest.

Acknowledgment. Parts of this research are supported by NanoSensoMach ERC advanced Grant No. 267574 under the EC FP7/2007–2013 program and the Volkswagen Foundation, Germany.

REFERENCES AND NOTES

1. Li, Q.; Luan, G.; Guo, Q.; Liang, J. A New Class of Homogeneous Nucleic Acid Probes Based on Specific Displacement Hybridization. *Nucleic Acids Res.* **2002**, *30*, e5.
2. Zhang, D. Y.; Seelig, G. Dynamic DNA Nanotechnology Using Strand-Displacement Reactions. *Nat. Chem.* **2011**, *3*, 103–113.
3. Collie, G. W.; Parkinson, G. N. The Application of DNA and RNA G-Quadruplexes to Therapeutic Medicines. *Chem. Soc. Rev.* **2011**, *40*, 5867–5892.
4. Davis, J. T.; Spada, G. P. Supramolecular Architectures Generated by Self-Assembly of Guanosine Derivatives. *Chem. Soc. Rev.* **2007**, *36*, 296–313.
5. Gehring, K.; Leroy, J. L.; Guéron, M. A Tetrameric DNA Structure with Protonated Cytosine–Cytosine Base Pairs. *Nature* **1993**, *363*, 561–565.
6. Miyake, Y.; Togashi, H.; Tashiro, M.; Yamaguchi, H.; Oda, S.; Kudo, M.; Tanaka, Y.; Kondo, Y.; Sawa, R.; Fujimoto, T.; *et al.* Mercury^{II}-Mediated Formation of Thymine-Hg^{II}-Thymine Base Pairs in DNA Duplexes. *J. Am. Chem. Soc.* **2006**, *128*, 2172–2173.
7. Ono, A.; Cao, S. Q.; Togashi, H.; Tashiro, M.; Fujimoto, T.; Machinami, T.; Oda, S.; Miyake, Y.; Okamoto, I.; Tanaka, Y. Specific Interactions Between Silver(I) Ions and Cytosine–Cytosine Pairs in DNA Duplexes. *Chem. Commun.* **2008**, 4825–4827.
8. Tuerk, C.; Gold, L. Systematic Evolution of Ligands by Exponential Enrichment: RNA Ligands to Bacteriophage T4 DNA Polymerase. *Science* **1990**, *249*, 505–510.
9. Ellington, A. D.; Szostak, J. W. *In Vitro* Selection of RNA Molecules that Bind Specific Ligands. *Nature* **1990**, *346*, 818–822.
10. Breaker, R. R.; Joyce, G. F. A DNA Enzyme that Cleaves RNA. *Chem. Biol.* **1994**, *1*, 223–229.
11. Willner, I.; Shlyahovsky, B.; Zayats, M.; Willner, B. DNAzymes for Sensing, Nanobiotechnology and Logic

Gate Applications. *Chem. Soc. Rev.* **2008**, *37*, 1153–1165.
12. Teller, C.; Willner, I. Organizing Protein-DNA Hybrids as Nanostructures with Programmed Functionalities. *Trends Biotechnol.* **2010**, *28*, 619–628.
13. Aldaye, F. A.; Palmer, A. L.; Sleiman, H. F. Assembling Materials with DNA as the Guide. *Science* **2008**, *321*, 1795–1799.
14. Liu, J.; Cao, Z.; Lu, Y. Functional Nucleic Acid Sensors. *Chem. Rev.* **2009**, *109*, 1948–1998.
15. Kolpashchikov, D. M. Binary Probes for Nucleic Acid Analysis. *Chem. Rev.* **2010**, *110*, 4709–4723.
16. Wang, F.; Willner, B.; Willner, I. DNA Nanotechnology with One-Dimensional Self-Assembled Nanostructures. *Curr. Opin. Biotechnol.* **2013**, *24*, 562–574.
17. Winfree, E.; Liu, F.; Wenzler, L. A.; Seeman, N. C. Design and Self-Assembly of Two-Dimensional DNA Crystals. *Nature* **1998**, *394*, 539–544.
18. Keren, K.; Krueger, M.; Gilad, R.; Ben-Yoseph, G.; Sivan, U.; Braun, E. Sequence-Specific Molecular Lithography on Single DNA Molecules. *Science* **2002**, *297*, 72–75.
19. Dittmer, W. U.; Reuter, A.; Simmel, F. C. A DNA-Based Machine that Can Cyclically Bind and Release Thrombin. *Angew. Chem., Int. Ed.* **2004**, *43*, 3550–3553.
20. Qian, L.; Winfree, E.; Bruck, J. Neural Network Computation with DNA Strand Displacement Cascades. *Nature* **2011**, *475*, 368–372.
21. Elbaz, J.; Wang, F.; Remacle, F.; Willner, I. pH-Programmable DNA Logic Arrays Powered by Modular DNAzyme Libraries. *Nano Lett.* **2012**, *12*, 6049–6054.
22. Li, D.; Song, S.; Fan, C. Target-Responsive Structural Switching for Nucleic Acid-Based Sensors. *Acc. Chem. Res.* **2010**, *43*, 631–641.
23. Douglas, S. M.; Bachelet, I.; Church, G. M. A Logic-Gated Nanorobot for Targeted Transport of Molecular Payloads. *Science* **2012**, *335*, 831–834.
24. Xiong, X.; Wu, C.; Zhou, C.; Zhu, G.; Chen, Z.; Tan, W. Responsive DNA-Based Hydrogels and Their Applications. *Macromol. Rapid Commun.* **2013**, *34*, 1271–1283.
25. Grieve, K.; Mulvaney, P.; Grieser, F. Synthesis and Electronic Properties of Semiconductor Nanoparticles/Quantum Dots. *Curr. Opin. Colloid Interface Sci.* **2000**, *5*, 168–172.
26. Alivisatos, P. The Use of Nanocrystals in Biological Detection. *Nat. Biotechnol.* **2004**, *22*, 47–52.
27. Gill, R.; Zayats, M.; Willner, I. Semiconductor Quantum Dots for Bioanalysis. *Angew. Chem., Int. Ed.* **2008**, *47*, 7602–7625.
28. Freeman, R.; Girsh, J.; Willner, I. Nucleic Acid/Quantum Dots (QDs) Hybrid Systems for Optical and Photoelectrochemical Sensing. *ACS Appl. Mater. Interfaces* **2013**, *5*, 2815–2834.
29. Xiao, Y.; Pavlov, V.; Niazov, T.; Dishon, A.; Kotler, M.; Willner, I. Catalytic Beacons for the Detection of DNA and Telomerase Activity. *J. Am. Chem. Soc.* **2004**, *126*, 7430–7431.
30. Pavlov, V.; Xiao, Y.; Gill, R.; Dishon, A.; Kotler, M.; Willner, I. Amplified Chemiluminescence Surface Detection of DNA and Telomerase Activity Using Catalytic Nucleic Acid Labels. *Anal. Chem.* **2004**, *76*, 2152–2156.
31. Pelossof, G.; Tel-Vered, R.; Willner, I. Amplified Surface Plasmon Resonance and Electrochemical Detection of Pb^{2+} Ions Using the Pb^{2+}-Dependent DNAzyme and Hemin/G-Quadruplex as a Label. *Anal. Chem.* **2012**, *84*, 3703–3709.
32. Freeman, R.; Liu, X.; Willner, I. Chemiluminescent and Chemiluminescence Resonance Energy Transfer (CRET) Detection of DNA, Metal Ions, and Aptamer-Substrate Complexes Using Hemin/G-Quadruplexes and CdSe/ZnS Quantum Dots. *J. Am. Chem. Soc.* **2011**, *133*, 11597–11604.
33. Liu, X.; Freeman, R.; Golub, E.; Willner, I. Chemiluminescence and Chemiluminescence Resonance Energy Transfer (CRET) Aptamer Sensors Using Catalytic Hemin/G-Quadruplexes. *ACS Nano* **2011**, *5*, 7648–7655.
34. Freeman, R.; Liu, X.; Willner, I. Amplified Multiplexed Analysis of DNA by the Exonuclease III-Catalyzed Regeneration of the Target DNA in the Presence of Functionalized Semiconductor Quantum Dots. *Nano Lett.* **2011**, *11*, 4456–4461.
35. Freeman, R.; Girsh, J.; Jou, A. F.; Ho, J. A.; Hug, T.; Dernedde, J.; Willner, I. Optical Aptasensors for the Analysis of the Vascular Endothelial Growth Factor (VEGF). *Anal. Chem.* **2012**, *84*, 6192–6198.
36. Choi, S.; Dickson, R. M.; Yu, J. Developing Luminescent Silver Nanodots for Biological Applications. *Chem. Soc. Rev.* **2012**, *41*, 1867–1891.
37. Liu, X.; Wang, F.; Aizen, R.; Yehezkeli, O.; Willner, I. Graphene Oxide/Nucleic-Acid-Stabilized Silver Nanoclusters: Functional Hybrid Materials for Optical Aptamer Sensing and Multiplexed Analysis of Pathogenic DNAs. *J. Am. Chem. Soc.* **2013**, *135*, 11832–11829.
38. Yurke, B.; Turberfield, A. J.; Mills, A. P.; Simmel, F. C., Jr.; Neumann, J. L. A DNA-Fuelled Molecular Machine Made of DNA. *Nature* **2000**, *406*, 605–608.
39. Elbaz, J.; Wang, Z. G.; Orbach, R.; Willner, I. pH-Stimulated Concurrent Mechanical Activation of Two DNA "Tweezers." A "SET-RESET" Logic Gate System. *Nano Lett.* **2009**, *9*, 4510–4514.
40. Wang, Z. G.; Elbaz, J.; Remacle, F.; Levine, R. D.; Willner, I. All-DNA Finite-State Automata with Finite Memory. *Proc. Natl. Acad. Sci. U.S.A.* **2010**, *107*, 21996–22001.
41. Liang, X.; Nishioka, H.; Takenaka, N.; Asanuma, H. A DNA Nanomachine Powered by Light Irradiation. *ChemBioChem* **2008**, *9*, 702–705.
42. Lund, K.; Manzo, A. J.; Dabby, N.; Michelotti, N.; Johnson-Buck, A.; Nangreave, J.; Taylor, S.; Pei, R.; Stojanovic, M. N.; Walter, N. G.; *et al.* Molecular Robots Guided by Prescriptive Landscapes. *Nature* **2010**, *465*, 206–210.
43. Wilner, O. I.; Willner, I. Functionalized DNA Nanostructures. *Chem. Rev.* **2012**, *112*, 2528–2556.
44. Modi, S.; G., S. M.; Goswami, D.; Gupta, G. D.; Mayor, S.; Krishnan, Y. A DNA Nanomachine that Maps Spatial and Temporal pH Changes Inside Living Cells. *Nat. Nanotechnol.* **2009**, *4*, 325–330.
45. Modi, S.; Nizak, C.; Surana, S.; Halder, S.; Krishnan, Y. Two DNA Nanomachines Map pH Changes Along Intersecting Endocytic Pathways Inside the Same Cell. *Nat. Nanotechnol.* **2013**, *8*, 459–467.
46. Mertens, H.; Koenderink, A. F.; Polman, A. Plasmon-Enhanced Luminescence Near Noble-Metal Nanospheres: Comparison of Exact Theory and an Improved Gersten and Nitzan Model. *Phys. Rev. B* **2007**, *76*, 115123.
47. Shimron, S.; Cecconello, A.; Lu, C. H.; Willner, I. Metal Nanoparticle-Functionalized DNA Tweezers: From Mechanically Programmed Nanostructures to Switchable Fluorescence Properties. *Nano Lett.* **2013**, *13*, 3791–3795.
48. Elbaz, J.; Cecconello, A.; Fan, Z.; Govorov, A. O.; Willner, I. Powering the Programmed Nanostructure and Function of Gold Nanoparticles with Catenated DNA Machines. *Nat. Commun.* **2013**, *4*, 2000.
49. Vallet-Regi, M.; Balas, F.; Arcos, D. Mesoporous Materials for Drug Delivery. *Angew. Chem., Int. Ed.* **2007**, *46*, 7548–7558.
50. Yang, Q.; Wang, S.; Fan, P.; Wang, L.; Di, Y.; Lin, K.; Xiao, F. S. pH-Responsive Carrier System Based on Carboxylic Acid Modified Mesoporous Silica and Polyelectrolyte for Drug Delivery. *Chem. Mater.* **2005**, *17*, 5999–6003.
51. Liu, N.; Dunphy, D. R.; Atanassov, P.; Bunge, S. D.; Chen, Z.; Lopez, G. P.; Boyle, T. J.; Brinker, C. J. Photoregulation of Mass Transport Through a Photoresponsive Azobenzene-Modified Nanoporous Membrane. *Nano Lett.* **2004**, *4*, 551–554.
52. Zhang, Z. X.; Balogh, D.; Wang, F.; Tel-Vered, R.; Levy, N.; Sung, S. Y.; Nechushtai, R.; Willner, I. Light-Induced and Redox-Triggered Uptake and Release of Substrates to and from Mesoporous SiO_2 Nanoparticles. *J. Mater. Chem. B* **2013**, *1*, 3159–3166.
53. Yu, A.; Wang, Y.; Barlow, E.; Caruso, F. Mesoporous Silica Particles as Templates for Preparing Enzyme-Loaded

Biocompatible Microcapsules. *Adv. Mater.* **2005**, *17*, 1737–1741.
54. Liong, M.; Lu, J.; Kovochich, M.; Xia, T.; Ruehm, S. G.; Nel, A. E.; Tamanoi, F.; Zink, J. I. Multifunctional Inorganic Nanoparticles for Imaging, Targeting, and Drug Delivery. *ACS Nano* **2008**, *2*, 889–896.
55. Zhao, Y.; Trewyn, B. G.; Slowing, I. I.; Lin, V. S. Y. Mesoporous Silica Nanoparticle-Based Double Drug Delivery System for Glucose-Responsive Controlled Release of Insulin and Cyclic AMP. *J. Am. Chem. Soc.* **2009**, *131*, 8398–8400.
56. Zhang, Z.; Balogh, D.; Wang, F.; Willner, I. Smart Mesoporous SiO_2 Nanoparticles for the DNAzyme-Induced Multiplexed Release of Substrates. *J. Am. Chem. Soc.* **2013**, *135*, 1934–1940.
57. Zhang, Z.; Balogh, D.; Wang, F.; Sung, S. Y; Nechushtai, R.; Willner, I. Biocatalytic Release of an Anti-Cancer Drug from Nucleic Acids-Capped Mesoporous SiO_2 Using DNA or Molecular Biomarkers as Triggering Stimuli. *ACS Nano* **2013**, 10.1021/nn403772j.